

# 1 Wall loss of semi-volatile organic compounds in a Teflon bag chamber 2 for the temperature range of 262-298 K: mechanistic insight on 3 temperature dependence

4 Longkun He<sup>1</sup>, Wenli Liu<sup>2</sup>, Yatai Li<sup>1,3</sup>, Jixuan Wang<sup>1</sup>, Mikinori Kuwata<sup>2</sup>, Yingjun Liu<sup>1</sup>

5 <sup>1</sup>State Key Joint Laboratory of Environmental Simulation and Pollution Control, College of Environmental Sciences and  
6 Engineering, Peking University, Beijing, 100871, China

7 <sup>2</sup>Department of Atmospheric and Oceanic Sciences and Laboratory for Climate and Ocean-Atmosphere Studies, School of  
8 Physics, Peking University, Beijing 100871, China

9 <sup>3</sup>Now at College of Public Health, Zhengzhou University, Zhengzhou, 450001, China

10 Correspondence to: Mikinori Kuwata ([kuwata@pku.edu.cn](mailto:kuwata@pku.edu.cn)), Yingjun Liu ([yingjun.liu@pku.edu.cn](mailto:yingjun.liu@pku.edu.cn))

11  
12 **Abstract.** Teflon bag chambers have long been used for investigating atmospheric chemical processes, including secondary  
13 organic aerosol formation. The wall-loss process of gas-phase species in Teflon bag chambers has typically been investigated  
14 at around room temperature. Recent laboratory studies started employing Teflon bag chambers at sub-273 K conditions for  
15 simulating wintertime and upper tropospheric environments. However, temperature dependence in vapor wall-loss processes  
16 of semi-volatile organic compounds (SVOCs) in a Teflon bag chamber has not well been investigated. In this study, we  
17 experimentally investigated wall-loss process of C<sub>14</sub>-C<sub>19</sub> *n*-alkanes in a 1 m<sup>3</sup> Teflon bag for the temperature range of 262 to  
18 298 K. Enhanced wall losses of the tested *n*-alkanes were observed following the decrease in temperature. For instance, 65%  
19 of C<sub>14</sub> *n*-alkane was lost to the wall 15 hours after injection at room temperature, while the corresponding value was 95% at  
20 262 K. The experimental data were analyzed using the two-layer kinetic model, which considers both absorption of gas phase  
21 species to the surface layer of Teflon wall and diffusion to the inner layer. The experimental data demonstrated that absorption  
22 of gas phase species by the surface layer enhanced at lower temperature. The temperature dependence in absorption was well  
23 accounted using the equilibrium dissolution model of organic compounds to the Teflon surface by considering reduced  
24 saturation vapor pressure at lower temperature. On the contrary, diffusion of *n*-alkanes from the surface to inner layer slowed  
25 down at reduced temperature. Mechanistic studies on these processes will need to be conducted in the future to quantitatively  
26 predict the influence of temperature-dependent wall-loss processes of SVOCs on laboratory experimental results.

## 27 **1 Introduction**

28           The environmental chamber is one of the most widely-used laboratory systems for studying chemical processes in  
29 the atmosphere, including formation of secondary organic aerosol (SOA) (Clark et al., 2016; Nakao et al., 2011; Ng et al.,  
30 2007; Song et al., 2005). The environmental chambers are typically made of Teflon films or stainless steel (Cocker et al., 2001;  
31 Voigtlaeander et al., 2012). Existence of walls in the environmental chambers induces losses of both vapors and particles due  
32 to their deposition on wall surfaces (McMurry and Grosjean, 1985; Krechmer et al., 2020). Wall loss of gas-phase organic  
33 compounds in the environmental chambers can lead to underestimation of SOA mass yields. For instance, injection of seed  
34 particles into Teflon bag has been shown to increase SOA yields by a few times due to the reduced relative importance of the  
35 chamber wall as a condensation sink in the system (Kroll et al., 2007; Zhang et al., 2014).

36           Vapor wall loss in Teflon bag chambers, especially that for semi-volatile organic compounds (SVOCs), has been  
37 intensively investigated in the last decade (Matsunaga and Ziemann, 2010; Yeh and Ziemann, 2014, 2015; Zhang et al., 2015;  
38 Krechmer et al., 2016; Huang et al., 2018b; Pratap et al., 2020; Yu et al., 2022). For instance, Matsunaga and Ziemann (2010)  
39 studied wall-loss process of alkanes, alkenes, alcohols, and ketones. These previous wall-loss experiments were dominantly  
40 conducted at around room temperature (293~303 K), as most of the chamber studies employed the corresponding temperature  
41 range (Hidy, 2019). The experimental results were often modeled by assuming equilibrium dissolution of the organic  
42 compounds into the Teflon film. A more recent study separately considered the surface and inner layer of the Teflon film for  
43 explaining the loss process more quantitatively (Huang et al., 2018b).

44           Recently, a growing number of environmental chamber experiments have been conducted at low temperatures to  
45 simulate wintertime/upper tropospheric conditions in laboratory (Huang et al., 2018a; Pratap et al., 2019; Quelever et al., 2019;  
46 Simon et al., 2020; Wang et al., 2022). For instance, some SOA formation experiments have been conducted for the  
47 temperature range down to 223 K using stainless steel chambers such as the Aerosol Interaction and Dynamics in the  
48 Atmosphere (AIDA) and Cosmics Leaving Outdoor Droplets (CLOUD) chambers (Huang et al., 2018a; Simon et al., 2020).  
49 Teflon bag chambers have also been employed for the temperature range down to 258 K (Kristensen et al., 2017; Deng et al.,  
50 2021). These studies demonstrate that temperature is an important parameter determining both mass yields and chemical  
51 composition of SOA. Vapor wall loss of SVOCs in the environmental chambers for the corresponding temperature range needs  
52 to be understood for better interpreting these experimental data in a quantitative way. So far only one group attempted to  
53 investigate vapor wall loss below room temperature, by measuring the size evolution of levoglucosan particles injected into a  
54 Teflon chamber (Pratap et al., 2020). However, the experimental results were confounded by slow evaporation of levoglucosan  
55 from particles at low temperatures.

56           This study investigated vapor wall loss of C<sub>14</sub>-C<sub>19</sub> *n*-alkanes in a Teflon chamber for the temperature range of 262 to  
57 298 K by monitoring the evolution of their gas-phase concentrations following a pulse release. The wall-loss process was

58 investigated as a function of temperature. The experimental results were analyzed using the two-layer kinetic model, which  
59 considers partitioning of gas phase SVOCs to the surface layer, as well as further diffusion to the inner layer. Temperature  
60 effects on the two processes were evaluated separately.

## 61 **2 Experimental**

### 62 **2.1 Teflon chamber experiments**

63 Figure 1 shows the experimental setup. The experiment was conducted using a fluorinated ethylene propylene (FEP)  
64 bag with the volume of 1 m<sup>3</sup>. The thickness of the FEP film for the bag was 75 μm. The dimension of the bag was 260 cm ×  
65 55 cm × 70 cm. The area to volume ratio of the chamber was 7.26 m<sup>-1</sup>. The chamber volume was experimentally validated by  
66 employing CO<sub>2</sub> as a tracer (Figure S1). The timescale for CO<sub>2</sub> to be well mixed in the bag after a pulse injection was  
67 approximately 30 mins (Figure S1). The bag was newly purchased for the experiment, meaning that it was employed for no  
68 other experiments. The bag was installed in a chest freezer (Type 2288, Nixue Inc.), which was equipped with an additional  
69 internal thermal insulation layer. Two fans were installed in the freezer (outside the bag) to facilitate mixing of air so that air  
70 temperature in the freezer was uniform. The temperature of the freezer was measured at 3 points using temperature sensors  
71 (Figure 1). Temporal variation of temperature was ± 0.5 K at 262 K.

72 Throughout the experiments, purified air was employed. The purified air was produced using a zero air generator  
73 (Model 747–30, AADCO Instruments, Inc.) and further purified using a hydrocarbon trap (BHT-2, Agilent Technologies, Inc.).  
74 Hydrocarbon concentration in the purified air was less than 5 ppbv. Relative humidity (RH) was less than 0.1%.

75 Solutions containing C<sub>14</sub> - C<sub>19</sub> *n*-alkanes (Konoscience Inc., > 98%) were prepared and injected into the chamber.  
76 Hexane (Fisher Chemical Co., HPLC grade) was employed as the solvent. The purities and saturation vapor pressures of all  
77 chemicals are given in Table S1. The solutions were injected to the chamber using a syringe pump (Fusion 200 Touch, Chemyx  
78 Inc.) and a nebulizer (TR-30-A1, Meinhard Inc.) through polytetrafluoroethylene (PTFE) tubing, as shown in Figure 1. The  
79 use of nebulizer expedited the evaporation of the solution.

80 Eight sets of wall-loss experiments were conducted in the temperature range of 262 to 298 K. Prior to each experiment,  
81 the chamber was heated to ~320 K and continuously flushed using purified air. The cleaning process lasted for 2~3 days until  
82 the concentration of investigated *n*-alkanes dropped to the background level. To start an experiment, the chamber was switched  
83 to batch mode and the solution was injected to the chamber at room temperature. The injection lasted for 13 mins, with a liquid  
84 flow rate of 100 μL min<sup>-1</sup>. The air flow rate of the nebulizer was 0.7 L min<sup>-1</sup>. The resulting initial concentrations (*C*<sub>0</sub>) of  
85 individual *n*-alkanes in the chamber ranged from 4 to 50 μg m<sup>-3</sup> assuming no wall loss, which were lower than 20% of their  
86 saturation concentrations under the corresponding experimental temperature to avoid particle formation. The solution used for  
87 low-temperature experiments (< 278 K) did not contain C<sub>18</sub> and C<sub>19</sub> *n*-alkanes to avoid formation of particles. For experiments

88 below room temperature, the cooling system of the freezer was turned on one hour after the completion of the injection. The  
89 operation procedure was employed to avoid homogeneous nucleation and subsequent condensational growth of aerosol  
90 particles. The validity of employing this post-cooled operation procedure was demonstrated by comparison with a pre-cooled  
91 chamber result at 270 K (Figure S2). Measurements using an optical particle counter (11-D, GRIMM Aerosol Technik Ainring,  
92 Germany) experimentally confirmed negligible abundance of aerosol particles in the chamber ( $< 0.5 \mu\text{g m}^{-3}$ ). It took  $\sim 3$  hours  
93 for the temperature in the freezer to drop to a stable level after injection (Figure S3). Although the air in the bag leaked out  
94 during experiments due to compression of the bag by its own weight, absence of intrusion of room air to the bag was confirmed  
95 by observing no changes in contaminant signals (Table S2). The gas-phase concentrations of *n*-alkanes were therefore  
96 unaffected by the changes in bag volume.

97 Concentrations of SVOCs in the chamber were quantified using the semi-volatile thermal desorption aerosol gas  
98 chromatograph (SV-TAG, Aerodyne Research Inc. & Aerosol Dynamic Inc., USA) (Zhao et al., 2013). The gas  
99 chromatography-mass spectrometer (GC-MS) (7890B, Agilent Technologies, Inc.) was employed for the system. Detailed  
100 descriptions of the SV-TAG operation and performance tests were presented in our previous papers (Li et al., 2022a; Li et al.,  
101 2022b). Herein, chamber air was sampled through  $\sim 1$  m long perfluoroalkoxy alkane (PFA) tubing (1/4 inch in diameter). Prior  
102 to sampling, the chamber air passed through the PFA tubing at  $0.5 \text{ L min}^{-1}$  for at least 20 min for passivating the tubing wall  
103 (Matsunaga and Ziemann, 2010). Samples were periodically collected for 5 min at  $4 \text{ L min}^{-1}$  for each time at 1-15 hours after  
104 injection. As the absence of particles was confirmed, only gas-phase SVOCs were sampled by the SV-TAG. The instrument  
105 response to *n*-alkanes was calibrated with standards before and after each experiment (Figure S4), utilizing the in-situ automatic  
106 injection system (Isaacman et al., 2011). The gas-phase concentrations of SVOCs were calculated from the measured quantity  
107 of SVOCs and sampled air volume.

## 108 **2.2 Kinetic model**

109 Herein we used a unified vapor wall-loss transport model developed by Huang et al. (2018b) to fit the experimental  
110 data. Figure 2 shows the concept of the model. Briefly, SVOCs partition between the gas phase and the surface of the FEP  
111 film. Subsequently, the absorbed SVOCs may diffuse to the inner layer of the film. As the thickness of the FEP film (75  $\mu\text{m}$ )  
112 is a couple of orders larger than that of the surface layer ( $\sim 5 \text{ nm}$ ) (Huang et al., 2018b), the inner layer is assumed as an  
113 infinite sink. As a result, the diffusion process of SVOCs from the inner layer to the film surface is ignored. A list of all the  
114 parameters is provided in Nomenclature. The governing equations without and with considering diffusion to the inner layer  
115 are presented below, respectively.

116 (1) Without considering the diffusion process in the inner layer, the wall loss process is solely controlled by  
117 partitioning of SVOCs between the gas phase and surface layer and can be described as follows

118 
$$\text{Gas phase} \xrightleftharpoons[k_{-1}]{k_1} \text{Surface} \quad (1)$$

119 where  $k_1$  and  $k_{-1}$  are forward and backward rate constants in the process. The corresponding first-order kinetic equations are

120 
$$\begin{aligned} \frac{dC_{gas}}{dt} &= -k_1 C_{gas} + k_{-1} C_{surface} \\ \frac{dC_{surface}}{dt} &= k_1 C_{gas} - k_{-1} C_{surface} \end{aligned} \quad (2)$$

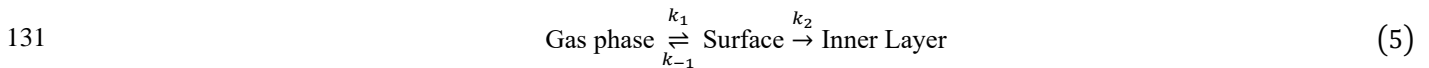
121 where  $C_{gas}$  and  $C_{surface}$  are the SVOC concentrations in gas phase and on wall surface, respectively. It should be noted that  
 122  $C_{surface}$  was defined as the total mass of SVOC ~~that was on wall surface~~ divided by the chamber volume, following previous  
 123 studies (Matsunaga and Ziemann, 2010; Yeh and Ziemann, 2014, 2015). This model has been commonly used to interpret  
 124 the experimental data of vapor wall loss in previous studies (Matsunaga and Ziemann, 2010; Yeh and Ziemann, 2014, 2015;  
 125 Zhang et al., 2015).

126 The gas-surface equilibrium time scale  $\tau_{surface}$  and equilibrium constant  $K_{eq}$  can be obtained by

127 
$$\tau_{surface} = \frac{1}{k_1 + k_{-1}} \quad (3)$$

128 
$$K_{eq} = \frac{k_1}{k_{-1}} = \left[ \frac{C_{surface}}{C_{gas}} \right]_{eq} \quad (4)$$

129 (2) Considering the diffusion process in the inner layer, the whole vapor wall loss process can be formulated as  
 130 follows



132 where  $k_2$  is the first-order loss rate constant in the diffusion process. Correspondingly, the kinetic processes for  $C_{gas}$  and  
 133  $C_{surface}$  can be described by the following equations

134 
$$\begin{aligned} \frac{dC_{gas}}{dt} &= -k_1 C_{gas} + k_{-1} C_{surface} \\ \frac{dC_{surface}}{dt} &= k_1 C_{gas} - k_{-1} C_{surface} - k_2 C_{surface} \end{aligned} \quad (6)$$

135 The diffusion process has the first-order decay time scale  $\tau_{inner}$  of  $\tau_{inner} = \frac{1}{k_2}$ . If  $k_2 \ll k_1 + k_{-1}$  (i.e.,  $\tau_{inner} \gg \tau_{surface}$ ),  
136 gas-surface partitioning occurs much faster than the diffusion process to the inner layer. In this case, the apparent first-order  
137 decay loss constant of SVOC from the gas phase can asymptotically be represented as (Huang et al., 2018b):

$$138 \quad \frac{dC_{gas}}{C_{gas}dt} \approx -\frac{K_{eq}}{1 + K_{eq}}k_2 \quad (7)$$

139 The data analysis and model fitting were conducted using Wolfram Mathematica 13.1. The controlling factors of  
140 individual parameters in the above equations were previously discussed by Huang et al. (2018b).

## 141 **3 Results and discussion**

### 142 **3.1 Wall loss of *n*-alkanes at room temperature**

143 An example of temporal profile for C<sub>14</sub>-C<sub>19</sub> *n*-alkanes during the experiment at 298 K is shown in Figure 3. The figure  
144 demonstrates the temporal change of  $C_{gas}/C_0$ , where  $C_0$  indicates the initial concentration of *n*-alkanes. The values of  $C_{gas}/C_0$   
145 for each *n*-alkane exhibited similar temporal patterns. During the first one hour following the injection,  $C_{gas}/C_0$  exponentially  
146 decreased. After that, gradual decreases in  $C_{gas}/C_0$  were observed. For example, the decline in gas fraction for C<sub>14</sub> *n*-alkane  
147 during the first hour accounted for 71% of the total change in  $C_{gas}/C_0$  over the whole experimental period of 15 hours. The  
148 values of  $C_{gas}/C_0$  decreased with the increase in carbon number, indicating enhanced wall loss. The values of  $C_{gas}/C_0$  at 15  
149 hours after injection were 0.32, 0.25, 0.16, 0.097, 0.069, and 0.037 for C<sub>14</sub> - C<sub>19</sub> *n*-alkanes, respectively.

150 The experimental result can be well fitted using the two-layer model, but the fits deteriorate in the case that diffusion  
151 in the inner layer is neglected (Figure 3). The optimized parameter sets are shown in Table S3. Mass fractions of injected  
152 chemical species in the gas, surface, and inner layer phases that were estimated using the model are shown in Figure S5. In the  
153 case of the most volatile compound (C<sub>14</sub> *n*-alkane), the maximum mass fraction in the surface phase occurred at 2 hours after  
154 injection. Subsequently, the mass fractions for the compound in both gas phase and surface layer gradually decreased. During  
155 this period, the ratio of the mass in the surface layer to that in the gas phase stabilized at 1.33. The mass fraction of the  
156 compound in the inner layer steadily increased, reaching 0.22 at 15 hours after injection.

157 In the case of the least volatile compound (C<sub>19</sub> *n*-alkane), the mass fraction in the surface layer reached the maximum  
158 (~76%) approximately 1 hour after injection, accounting for the rapid decrease in the observed concentration in the gas phase.  
159 Subsequently, mass fractions of the compound in the gas phase and in the surface layer decreased in proportion. The  
160 concentration ratio of the gas phase and surface layer ~~was maintained as~~ stayed constant (Figure S5). The mass fraction of

161 the compound in the inner layer kept increasing during the experiment. At 15 hours after injection, 87% of the compound  
162 existed in the inner layer.

163 The time scale for *n*-alkanes to reach partitioning equilibrium between the gas and surface phases is estimated to be  
164 12 ~ 35 mins, consistent with literature data. For example, Matsunaga and Ziemann (2010) reported that the corresponding  
165 time scale for C<sub>8</sub> - C<sub>16</sub> alkanes was 60 ± 20 mins. The corresponding value for oxygenated organic compounds was reported  
166 as 26 ± 23 mins (Yeh and Ziemann, 2015).

167 Our result for the mass transfer of SVOCs to the inner layer can also be compared with a previous study. The rates  
168 for the decrease in  $C_{gas}/C_0$  for C<sub>14</sub>-C<sub>19</sub> *n*-alkanes were 0.6–1.3% hour<sup>-1</sup> after the partitioning between gas phase and surface  
169 layer reached equilibrium (*i.e.*, 3 ~ 15 hours). Yeh and Ziemann (2015) reported the corresponding value for 2-ketones as  
170 approximately 1% hour<sup>-1</sup> for the time scale of 7 hours. They suggested that the value is close to the theoretical value for the  
171 Fickian diffusion loss rate (~0.5 % hour<sup>-1</sup>).

### 172 3.2 Temperature dependence of wall loss of *n*-alkanes

173 Figure 4a summarizes the values of  $C_{gas}/C_0$  for all experiments at 3 hours after injection. The data for this sampling  
174 time ~~was/were~~ selected, as the loss of gas phase species by partitioning to the surface layer accounted for the dominant portion  
175 of the decline in the gas phase concentration. ~~It should be noted that fitting the experimental data using the two-layer model  
176 was challenging for the low-temperature experiments. Since the chamber was cooled after the injection of *n*-alkanes, the model  
177 parameters would change correspondingly with chamber temperature. Potential uncertainties associated with the employment  
178 of the data at 3 hours after injection as a proxy for gas-surface partitioning are summarized in Text S1.~~

179 ——— Generally,  $C_{gas}/C_0$  was lower for less volatile compounds and at lower temperature, suggesting enhanced partitioning  
180 of *n*-alkanes to the chamber wall. The data for the room temperature ( $C_{gas}/C_0 = 0.47, 0.45, 0.34, 0.24, 0.17,$  and  $0.091$  for C<sub>14</sub>,  
181 C<sub>15</sub>, C<sub>16</sub>, C<sub>17</sub>, C<sub>18</sub>, and C<sub>19</sub> *n*-alkanes) were smaller than that have been reported by a previous study. Namely, Matsunaga and  
182 Ziemann (2010) quantified the corresponding values for equilibration between the gas and surface phases for C<sub>14</sub>-C<sub>16</sub> *n*-alkanes  
183 as ~80–90%. The enhanced partitioning to the surface layer in our study is likely due to that the chamber for the present study  
184 has a larger area to volume ratio (7.26 m<sup>-1</sup> versus 3.39 m<sup>-1</sup>).

185 Figure 4b shows the values of  $C_{gas}/C_0$  as a function of temperature at 15 hours after injection. In all experiments, the  
186 values of  $C_{gas}/C_0$  at 15 hours after injection were consistently lower than those for 3 hours. For instance,  $C_{gas}/C_0$  for C<sub>14</sub> *n*-  
187 alkane at 262 K decreased from 0.15 (3 hours) to 0.06 (15 hours). As discussed in the case of the experiment at 298 K, the  
188 result suggests that diffusional loss in the inner layer of the chamber wall occurred for the whole temperature range.

### 189 3.3 Temperature dependence of partitioning between gas phase and wall surface

190 The temperature dependence in the data summarized in Figure 4a can be understood by considering changes in  
191 partitioning between the gas phase and surface layer. Matsunaga and Ziemann (2010) introduced the following equation for  
192 relating  $C_{surface}/C_{gas}$  and temperature based on the equilibrium dissolution model:

$$193 \left[ \frac{C_{surface}}{C_{gas}} \right]_{eq} = K_{eq} = \frac{C_{FEP\_surface}RT}{M_{wall}\gamma_{FEP\_surface}P_s(T)} \quad (8)$$

194 where  $C_{FEP\_surface}$  is the equivalent organic mass concentration of the FEP chamber surface wall,  $M_{wall}$  is the average  
195 molecular mass of the FEP,  $\gamma_{FEP\_surface}$  is the activity coefficient of the organic compound in the Teflon surface,  $R$  is the gas  
196 constant, and  $T$  is temperature.  $P_s(T)$  is the saturation vapor pressure of the compound at temperature  $T$ . Among the terms for  
197 the right-hand-side of equation (8),  $RT/P_s(T)$  can be calculated from the experimental conditions. Herein~~To use Equation (8)~~  
198  $P_s(T)$  was calculated by the EVAPORATION group contribution method (Comperolle et al., 2011). Comparison between  
199 the EVAPORATION method withand other approaches for estimating  $P_s(T)$  is available in Figure S6. The equation suggests  
200 that  $[C_{surface}/C_{gas}]_{eq}$  and  $RT/P_s(T)$  may vary in proportion, with the slope of  $C_{FEP\_surface}/(M_{wall}\gamma_{FEP\_surface})$ .

201 It is challenging to retrieve the value of  $[C_{surface}/C_{gas}]_{eq}$  by fitting the data of the low-temperature experiments  
202 using the two-layer model, since the chamber was cooled after the injection of  $n$ -alkanes. Alternatively, ~~The~~ ~~the~~ value of  
203  $[C_{surface}/C_{gas}]_{eq}$  was approximated using  $1/[C_{gas}/C_0]_{at\ 3\ hours} - 1$ , ~~by~~ assuming that diffusion of  $n$ -alkanes to the inner layer  
204 was still a minor loss process within 3 hours. ~~Potential uncertainties associated with this approximation are summarized in~~  
205 Text S1. The uncertainties were estimated in two ways: (1) kinetic simulation based on fitting parameters in Figure 3 (Figure  
206 S5) and (2) comparison of the retrieved values of  $[C_{surface}/C_{gas}]_{eq}$  (i.e.,  $K_{eq}$ ) and  $1/[C_{gas}/C_0]_{at\ 3\ hours} - 1$  at room  
207 temperature (Table S3). The room-temperature experiments were conducted for three runs, allowing for the estimation of  
208 experimental uncertainties as standard deviation. Although the kinetic simulation implies overestimates of 7 - 55%, the  
209 measurement-based comparison demonstrates that  $1/[C_{gas}/C_0]_{at\ 3\ hours} - 1$  and  $[C_{surface}/C_{gas}]_{eq}$  agreed within the  
210 experimental uncertainties, thereby supporting the validity of the approximation.

211 Figure 5 shows the correlations between  $C_{surface}/C_{gas}$  and  $RT/P_s(T)$  for individual compounds. For all the tested  
212 compounds, these two parameters correlated well, even though  $C_{surface}/C_{gas}$  increased by more than one order of magnitude  
213 when the chamber was cooled down. The result suggests that equation (8) can be applied to a wide range of temperatures  
214 without considering the temperature dependence of  $C_{FEP\_surface}/(M_{wall}\gamma_{FEP\_surface})$  ~~to account for partitioning of  $n$  alkanes~~  
215 ~~to the surface layer~~. In other word,  $\gamma_{FEP\_surface}$  can be practically treated as a constant for the investigated temperature range,



216 given  $C_{FEP\_surface}$  and  $M_{wall}$  are independent of temperature. This implication is consistent with previous findings that the  
217 activity coefficients of organic compounds in polymers only change slightly with temperature. For instance, Kontogeorgis et  
218 al. (1993) compared the experimental and modelled values of activity coefficients for hydrocarbons in a few polymers such as  
219 low-density polyethylene. The values of activity coefficients change by 10~20% for a temperature change of 100 K. ~~Further  
220 studies, that employ different chemical species, would be needed in the future for validating and applying the relation to a  
221 wider range.~~

222 Values of  $\gamma_{FEP\_surface}$  for *n*-alkanes can be estimated from Figure 5. Based on equation (8), the fitted slopes  
223 correspond to  $C_{FEP\_surface}/(M_{wall}\gamma_{FEP\_surface})$ . For a specific chamber design, compound-independent  $C_{FEP\_surface}$  can be  
224 estimated by the density of FEP film ( $2150\text{ kg m}^{-3}$ ) ~~and the thickness of surface layer ( $\sim 5\text{ nm}$ ), and the surface-to-volume  
225 ratio of the chamber~~ (Huang et al., 2018b). ~~For the chamber in this experiment, The estimated  $C_{FEP\_surface}$  for the chamber in  
226 this experiment was assumed as  $78.2\text{ mg m}^{-3}$ , following the recommendation by Huang et al. (2018b).~~ For estimating  
227 compound-dependent  $\gamma_{FEP\_surface}$ , previous studies assumed  $M_{wall} = 200\text{ g mol}^{-1}$  (Huang et al., 2018b; Matsunaga and  
228 Ziemann, 2010). The same approximations were employed in the present study.

229 Figure 6 plots the retrieved values of  $\gamma_{FEP\_surface}$  for *n*-alkanes against  $P_s(298\text{ K})$  for *n*-alkanes. The figure also  
230 shows the corresponding parameters obtained from previous experimental studies (compiled by Huang et al. (2018b), including  
231 Matsunaga and Ziemann (2010), Yeh and Ziemann (2014, 2015), and Krechmer et al. (2016)). It should be noted that the  
232 literature results were analyzed with fixed values of area to volume ratio of  $3\text{ m}^{-1}$  and  $C_{FEP\_surface}$  of  $32.2\text{ mg m}^{-3}$  (Huang et  
233 al., 2018b). Regardless of differences in types of chemicals and chambers, the experimentally estimated values of  $\gamma_{FEP\_surface}$   
234 and  $P_s(298\text{ K})$  correlate in logarithmic scale. The relationship followed the equation of  $\ln(\gamma_{FEP\_surface}) = 0.40 -$   
235  $0.61\ln(P_s(298\text{ K}))$ .

### 236 3.4 Characterization of diffusion from the Teflon surface to inner layer

237 Values of  $k_2$  were estimated using equation (7), since values of  $\tau_{inner}$  are at least 18 times larger than those of  
238  $\tau_{surface}$  (Table S3). The values of  $C_{gas}/C_0$  at 3 hours after injection were employed to calculate  $K_{eq}$  as discussed earlier.  
239 The experimental data for 9, 12, and 15 hours after injection was employed for obtaining  $k_2$ .

240 Figure 7 plots the estimated values of  $k_2$  against  $P_s(T)$  for all compounds in all experiments. The values of  $k_2$  and  
241  $P_s(T)$  positively correlate. As a comparison point, a previous study reported positive correlations for (1) the diffusivity of  
242 organic compounds in FEP film and saturation concentration, and (2)  $k_2$  and diffusivity (Huang et al., 2018b). Our current  
243 result is qualitatively similar to the previous study, though temperature was maintained as a constant in the previous study.  
244 The decrease in  $k_2$  at lower temperature could be induced by reduced viscosity in the inner layer or weakened thermal motion  
245 of *n*-alkane molecules (Mattila et al., 2023). It should be noted that compression of bag volume during experiment would lead

246 to an increase in the area to volume ratio. Consequently, this could disrupt the relatively slow diffusion process. Based on  
247 some photos during the experiment, the leak-out air could have increased the area to volume ratio by a few ~~factor~~times.  
248 Further study, that ~~incorporates considering~~considers changes of chamber volume, would be needed in the future for  
249 quantitatively interpreting the data.

#### 250 4 Conclusions

251 The present study investigated the wall loss process of C<sub>14</sub>-C<sub>19</sub> *n*-alkanes to the wall of a 1 m<sup>3</sup> chamber bag, which was  
252 composed of FEP film. The temperature of the chamber was controlled for the range of 262 to 298 K. Decay in gas-phase  
253 concentrations of the *n*-alkanes was quantified using the SV-TAG for 15 hours following injection. The temporal variations in  
254 the *n*-alkane concentrations suggested two types of loss processes. The first process was characterized by rapid exponential  
255 decay in the first few hours. Subsequently, slow first-order decreases in the *n*-alkane concentrations ~~were~~was identified until  
256 the end of the experiment. Enhanced wall loss was observed at lower temperatures for all compounds.

257 The experimental data were well fitted using the two-layer kinetic model, which considers partitioning of gas-phase  
258 species to the surface layer of the chamber film and further diffusion to the inner layer. The analysis suggests that when the  
259 Teflon bag chamber is operated at low temperatures, partitioning of gas phase species to the chamber wall surface is enhanced,  
260 whereas the permeation of the chemical compounds to the inner layer is suppressed. The temperature effect on gas-surface  
261 partitioning overweighs that on diffusion into the inner layer for *n*-alkanes, leading to an overall enhanced wall loss at lower  
262 temperature.

263 The quasi-equilibrium partitioning of *n*-alkanes between the gas phase and surface layer was interpreted by considering  
264 the dissolution process of the species into the surface layer. Values of  $C_{surface}/C_{gas}$  at quasi-equilibrium are proportional to  
265  $RT/P_s(T)$  for individual compounds. The result suggests that decreased saturation vapor pressure is the major driving force  
266 for enhanced partitioning to the surface layer at low temperatures for all investigated compounds, while their activity  
267 coefficients can be practically treated as constants for the investigated temperature range. The relationship can be potentially  
268 employed for predicting changes in wall loss of SVOCs as a function of temperature, after further verification employing other  
269 types of organic compounds.

270 In the future, the underlying mechanisms of the present findings will need to be sought for a better understanding of the  
271 chamber wall loss of SVOCs. The present study focused on *n*-alkanes. In the case of chamber experiments for SOA formation,  
272 wall loss processes of oxygenated chemical species would be more important. Thus, a temperature-dependent wall loss study  
273 for oxygenated chemical species will still need to be conducted for interpreting SOA chamber experiments under a wide range  
274 of temperatures.

275 **Data Availability**

276 Data will be made available on request.

277 **Author contribution**

278 **Longkun He:** Conceptualization, Methodology, Experiment, Data curation, Formal analysis, Writing – original draft. **Wenli**  
279 **Liu:** Methodology, Experiment, Writing – review & editing. **Yatai Li:** Methodology, Writing – review & editing. **Jixuan**  
280 **Wang:** Experiment, Writing – review & editing. **Mikinori Kuwata:** Conceptualization, Methodology, Project administration,  
281 Funding acquisition, Formal analysis, Writing – review & editing, Supervision. **Yingjun Liu:** Conceptualization,  
282 Methodology, Project administration, Funding acquisition, Formal analysis, Writing – review & editing, Supervision.

283 **Competing interests**

284 The authors declare that they have no conflict of interest.

285 **Acknowledgements**

286 We thank Dr. Ying Zhou for assisting to improve figure quality. This research was supported by the National Natural  
287 Science Foundation of China (92044303, 42175121, and 42150610485).

288 **Reference**

- 289 Clark, C. H., Kacarab, M., Nakao, S., Asa-Awuku, A., Sato, K., and Cocker, D. R., III: Temperature effects on secondary  
290 organic aerosol (SOA) from the dark ozonolysis and photo-oxidation of isoprene, *Environ. Sci. Technol.*, 50, 5564-5571,  
291 <https://doi.org/10.1021/acs.est.5b05524>, 2016.
- 292 Cocker, D. R., Flagan, R. C., and Seinfeld, J. H.: State-of-the-art chamber facility for studying atmospheric aerosol chemistry,  
293 *Environ. Sci. Technol.*, 35, 2594-2601, <https://doi.org/10.1021/es0019169>, 2001.
- 294 Compernolle, S., Ceulemans, K., and Muller, J. F.: EVAPORATION: A new vapour pressure estimation method for organic  
295 molecules including non-additivity and intramolecular interactions, *Atmos. Chem. Phys.*, 11, 9431-9450,  
296 <https://doi.org/10.5194/acp-11-9431-2011>, 2011.
- 297 Deng, Y. G., Inomata, S., Sato, K., Ramasamy, S., Morino, Y., Enami, S., and Tanimoto, H.: Temperature and acidity  
298 dependence of secondary organic aerosol formation from alpha-pinene ozonolysis with a compact chamber system,  
299 *Atmos. Chem. Phys.*, 21, 5983-6003, <https://doi.org/10.5194/acp-21-5983-2021>, 2021.
- 300 Hidy, G. M.: Atmospheric chemistry in a box or a bag, *Atmosphere*, 10, 401, <https://doi.org/10.3390/atmos10070401>, 2019.
- 301 Huang, W., Saathoff, H., Pajunoja, A., Shen, X. L., Naumann, K. H., Wagner, R., Virtanen, A., Leisner, T., and Mohr, C.:  
302 Alpha-pinene secondary organic aerosol at low temperature: Chemical composition and implications for particle viscosity,  
303 *Atmos. Chem. Phys.*, 18, 2883-2898, <https://doi.org/10.5194/acp-18-2883-2018>, 2018a.
- 304 Huang, Y. L., Zhao, R., Charan, S. M., Kenseth, C. M., Zhang, X., and Seinfeld, J. H.: Unified theory of vapor-wall mass  
305 transport in Teflon-walled environmental chambers, *Environ. Sci. Technol.*, 52, 2134-2142,  
306 <https://doi.org/10.1021/acs.est.7b05575>, 2018b.
- 307 Isaacman, G., Kreisberg, N. M., Worton, D. R., Hering, S. V., and Goldstein, A. H.: A versatile and reproducible automatic  
308 injection system for liquid standard introduction: Application to in-situ calibration, *Atmos. Meas. Tech.*, 4, 1937-1942,  
309 <https://doi.org/10.5194/amt-4-1937-2011>, 2011.
- 310 Kontogeorgis, G. M., Fredenslund, A., and Tassios, D. P.: Simple activity-coefficient model for the prediction of solvent  
311 activities in polymer-solutions, *Ind. Eng. Chem. Res.*, 32, 362-372, <https://doi.org/10.1021/ie00014a013>, 1993.
- 312 Krechmer, J. E., Day, D. A., and Jimenez, J. L.: Always lost but never forgotten: Gas-phase wall losses are important in all  
313 Teflon environmental chambers, *Environ. Sci. Technol.*, 54, 12890-12897, <https://doi.org/10.1021/acs.est.0c03381>, 2020.
- 314 Krechmer, J. E., Pagonis, D., Ziemann, P. J., and Jimenez, J. L.: Quantification of gas-wall partitioning in Teflon environmental  
315 chambers using rapid bursts of low-volatility oxidized species generated in situ, *Environ. Sci. Technol.*, 50, 5757-5765,  
316 <https://doi.org/10.1021/acs.est.6b00606>, 2016.
- 317 Kristensen, K., Jensen, L. N., Glasius, M., and Bilde, M.: The effect of sub-zero temperature on the formation and composition  
318 of secondary organic aerosol from ozonolysis of alpha-pinene, *Environ. Sci.-Proc. Imp.*, 19, 1220-1234,  
319 <https://doi.org/10.1039/c7em00231a>, 2017.

320 Kroll, J. H., Chan, A. W. H., Ng, N. L., Flagan, R. C., and Seinfeld, J. H.: Reactions of semivolatile organics and their effects  
321 on secondary organic aerosol formation, *Environ. Sci. Technol.*, 41, 3545-3550, <https://doi.org/10.1021/es062059x>, 2007.

322 Li, Y. T., He, L. K., Xie, D., Zhao, A. Q., Wang, L. X., Kreisberg, N. M., Jayne, J., and Liu, Y. J.: Strong temperature influence  
323 and indiscernible ventilation effect on dynamics of some semivolatile organic compounds in the indoor air of an office,  
324 *Environ. Int.*, 165, 107305, <https://doi.org/10.1016/j.envint.2022.107305>, 2022a.

325 Li, Y. T., Xie, D., He, L. K., Zhao, A. Q., Wang, L. X., Kreisberg, N. M., Jayne, J., and Liu, Y. J.: Dynamics of di-2-ethylhexyl  
326 phthalate (DEHP) in the indoor air of an office, *Build. Environ.*, 223, 109446,  
327 <https://doi.org/10.1016/j.buildenv.2022.109446>, 2022b.

328 Matsunaga, A. and Ziemann, P. J.: Gas-wall partitioning of organic compounds in a Teflon film chamber and potential effects  
329 on reaction product and aerosol yield measurements, *Aerosol Sci. Technol.*, 44, 881-892,  
330 <https://doi.org/10.1080/02786826.2010.501044>, 2010.

331 Mattila, J. M., Li, E. Y., and Offenberg, J. H.: Tubing material considerably affects measurement delays of gas-phase  
332 oxygenated per- and polyfluoroalkyl substances, *J. Air Waste Manage. Assoc.*, 73, 335-344,  
333 <https://doi.org/10.1080/10962247.2023.2174612>, 2023.

334 McMurry, P. H. and Grosjean, D.: Gas and aerosol wall losses in Teflon film smog chambers, *Environ. Sci. Technol.*, 19,  
335 1176-1182, <https://doi.org/10.1021/es00142a006>, 1985.

336 Nakao, S., Shrivastava, M., Anh, N., Jung, H., and Cocker, D., III: Interpretation of secondary organic aerosol formation from  
337 diesel exhaust photooxidation in an environmental chamber, *Aerosol Sci. Technol.*, 45, 964-972,  
338 <https://doi.org/10.1080/02786826.2011.573510>, 2011.

339 Ng, N. L., Chhabra, P. S., Chan, A. W. H., Surratt, J. D., Kroll, J. H., Kwan, A. J., McCabe, D. C., Wennberg, P. O., Sorooshian,  
340 A., Murphy, S. M., Dalleska, N. F., Flagan, R. C., and Seinfeld, J. H.: Effect of NO<sub>x</sub> level on secondary organic aerosol  
341 (SOA) formation from the photooxidation of terpenes, *Atmos. Chem. Phys.*, 7, 5159-5174, [https://doi.org/10.5194/acp-](https://doi.org/10.5194/acp-7-5159-2007)  
342 [7-5159-2007](https://doi.org/10.5194/acp-7-5159-2007), 2007.

343 Pratap, V., Bian, Q. J., Kiran, S. A., Hopke, P. K., Pierce, J. R., and Nakao, S.: Investigation of levoglucosan decay in wood  
344 smoke smog-chamber experiments: The importance of aerosol loading, temperature, and vapor wall losses in interpreting  
345 results, *Atmos. Environ.*, 199, 224-232, <https://doi.org/10.1016/j.atmosenv.2018.11.020>, 2019.

346 Pratap, V., Kiran, S. A., Bian, Q., Pierce, J. R., Hopke, P. K., and Nakao, S.: Observation of vapor wall deposition in a smog  
347 chamber using size evolution of pure organic particles, *Aerosol Air Qual. Res.*, 20, 2705-2714,  
348 <https://doi.org/10.4209/aaqr.2020.05.0268>, 2020.

349 Quelever, L. L. J., Kristensen, K., Jensen, L. N., Rosati, B., Teiwes, R., Daellenbach, K. R., Perakyla, O., Roldin, P., Bossi,  
350 R., Pedersen, H. B., Glasius, M., Bilde, M., and Ehn, M.: Effect of temperature on the formation of highly oxygenated  
351 organic molecules (HOMs) from alpha-pinene ozonolysis, *Atmos. Chem. Phys.*, 19, 7609-7625,  
352 <https://doi.org/10.5194/acp-19-7609-2019>, 2019.

353 Simon, M., Dada, L., Heinritzi, M., Scholz, W., Stolzenburg, D., Fischer, L., Wagner, A. C., Kurten, A., Rorup, B., He, X. C.,  
354 Almeida, J., Baalbaki, R., Baccarini, A., Bauer, P. S., Beck, L., Bergen, A., Bianchi, F., Brakling, S., Brilke, S., Caudillo,  
355 L., Chen, D. X., Chu, B. W., Dias, A., Draper, D. C., Duplissy, J., El-Haddad, I., Finkenzeller, H., Frege, C., Gonzalez-  
356 Carracedo, L., Gordon, H., Granzin, M., Hakala, J., Hofbauer, V., Hoyle, C. R., Kim, C., Kong, W. M., Lamkaddam, H.,  
357 Lee, C. P., Lehtipalo, K., Leiminger, M., Mai, H. J., Manninen, H. E., Marie, G., Marten, R., Mentler, B., Molteni, U.,  
358 Nichman, L., Nie, W., Ojdanic, A., Onnela, A., Partoll, E., Petaja, T., Pfeifer, J., Philippov, M., Quelever, L. L. J.,  
359 Ranjithkumar, A., Rissanen, M. P., Schallhart, S., Schobesberger, S., Schuchmann, S., Shen, J. L., Sipila, M., Steiner, G.,  
360 Stozhkov, Y., Tauber, C., Tham, Y. J., Tome, A. R., Vazquez-Pufleau, M., Vogel, A. L., Wagner, R., Wang, M. Y., Wang,  
361 D. S., Wang, Y. H., Weber, S. K., Wu, Y. S., Xiao, M., Yan, C., Ye, P. L., Ye, Q., Zauner-Wieczorek, M., Zhou, X. Q.,  
362 Baltensperger, U., Dommen, J., Flagan, R. C., Hansel, A., Kulmala, M., Volkamer, R., Winkler, P. M., Worsnop, D. R.,  
363 Donahue, N. M., Kirkby, J., and Curtius, J.: Molecular understanding of new-particle formation from alpha-pinene  
364 between -50 and +25 °C, *Atmos. Chem. Phys.*, 20, 9183-9207, <https://doi.org/10.5194/acp-20-9183-2020>, 2020.

365 Song, C., Na, K. S., and Cocker, D. R.: Impact of the hydrocarbon to NO<sub>x</sub> ratio on secondary organic aerosol formation,  
366 *Environ. Sci. Technol.*, 39, 3143-3149, <https://doi.org/10.1021/es0493244>, 2005.

367 Voigtlaeander, J., Duplissy, J., Rondo, L., Kuerten, A., and Stratmann, F.: Numerical simulations of mixing conditions and  
368 aerosol dynamics in the CERN CLOUD chamber, *Atmos. Chem. Phys.*, 12, 2205-2214, [https://doi.org/10.5194/acp-12-](https://doi.org/10.5194/acp-12-2205-2012)  
369 [2205-2012](https://doi.org/10.5194/acp-12-2205-2012), 2012.

370 Wang, M. Y., Xiao, M., Bertozzi, B., Marie, G., Rorup, B., Schulze, B., Bardakov, R., He, X. C., Shen, J. L., Scholz, W.,  
371 Marten, R., Dada, L., Baalbaki, R., Lopez, B., Lamkaddam, H., Manninen, H. E., Amorim, A., Ataei, F., Bogert, P.,  
372 Brasseur, Z., Caudillo, L., De Menezes, L. P., Duplissy, J., Ekman, A. M. L., Finkenzeller, H., Carracedo, L. G., Granzin,  
373 M., Guida, R., Heinritzi, M., Hofbauer, V., Hohler, K., Korhonen, K., Krechmer, J. E., Kurten, A., Lehtipalo, K., Mahfouz,  
374 N. G. A., Makhmutov, V., Massabo, D., Mathot, S., Mauldin, R. L., Mentler, B., Muller, T., Onnela, A., Petaja, T.,  
375 Philippov, M., Piedehierro, A. A., Pozzer, A., Ranjithkumar, A., Schervish, M., Schobesberger, S., Simon, M., Stozhkov,  
376 Y., Tome, A., Umo, N. S., Vogel, F., Wagner, R., Wang, D. S., Weber, S. K., Welti, A., Wu, Y. S., Zauner-Wieczorek,  
377 M., Sipila, M., Winkler, P. M., Hansel, A., Baltensperger, U., Kulmala, M., Flagan, R. C., Curtius, J., Riipinen, I., Gordon,  
378 H., Lelieveld, J., El-Haddad, I., Volkamer, R., Worsnop, D. R., Christoudias, T., Kirkby, J., Mohler, O., and Donahue, N.  
379 M.: Synergistic HNO<sub>3</sub>-H<sub>2</sub>SO<sub>4</sub>-NH<sub>3</sub> upper tropospheric particle formation, *Nature*, 605, 483-489,  
380 <https://doi.org/10.1038/s41586-022-04605-4>, 2022.

381 Yeh, G. K. and Ziemann, P. J.: Alkyl nitrate formation from the reactions of C<sub>8</sub>-C<sub>14</sub> n-alkanes with OH radicals in the presence  
382 of NO<sub>x</sub>: Measured yields with essential corrections for gas-wall partitioning, *J. Phys. Chem. A*, 118, 8147-8157,  
383 <https://doi.org/10.1021/jp500631v>, 2014.

384 Yeh, G. K. and Ziemann, P. J.: Gas-wall partitioning of oxygenated organic compounds: Measurements, structure-activity  
385 relationships, and correlation with gas chromatographic retention factor, *Aerosol Sci. Technol.*, 49, 726-737,  
386 <https://doi.org/10.1080/02786826.2015.1068427>, 2015.

387 Yu, S., Jia, L., Xu, Y., Zhang, H., Zhang, Q., and Pan, Y.: Wall losses of oxygenated volatile organic compounds from  
388 oxidation of toluene: Effects of chamber volume and relative humidity, *J. Environ. Sci.*, 114, 475-484,  
389 <https://doi.org/10.1016/j.jes.2021.09.026>, 2022.

390 Zhang, X., Cappa, C. D., Jathar, S. H., McVay, R. C., Ensberg, J. J., Kleeman, M. J., and Seinfeld, J. H.: Influence of vapor  
391 wall loss in laboratory chambers on yields of secondary organic aerosol, *Proc. Natl. Acad. Sci. U. S. A.*, 111, 5802-5807,  
392 <https://doi.org/10.1073/pnas.1404727111>, 2014.

393 Zhang, X., Schwantes, R. H., McVay, R. C., Lignell, H., Coggon, M. M., Flagan, R. C., and Seinfeld, J. H.: Vapor wall  
394 deposition in Teflon chambers, *Atmos. Chem. Phys.*, 15, 4197-4214, <https://doi.org/10.5194/acp-15-4197-2015>, 2015.

395 Zhao, Y. L., Kreisberg, N. M., Worton, D. R., Teng, A. P., Hering, S. V., and Goldstein, A. H.: Development of an in situ  
396 thermal desorption gas chromatography instrument for quantifying atmospheric semi-volatile organic compounds,  
397 *Aerosol Sci. Technol.*, 47, 258-266, <https://doi.org/10.1080/02786826.2012.747673>, 2013.

398 **Nomenclature**

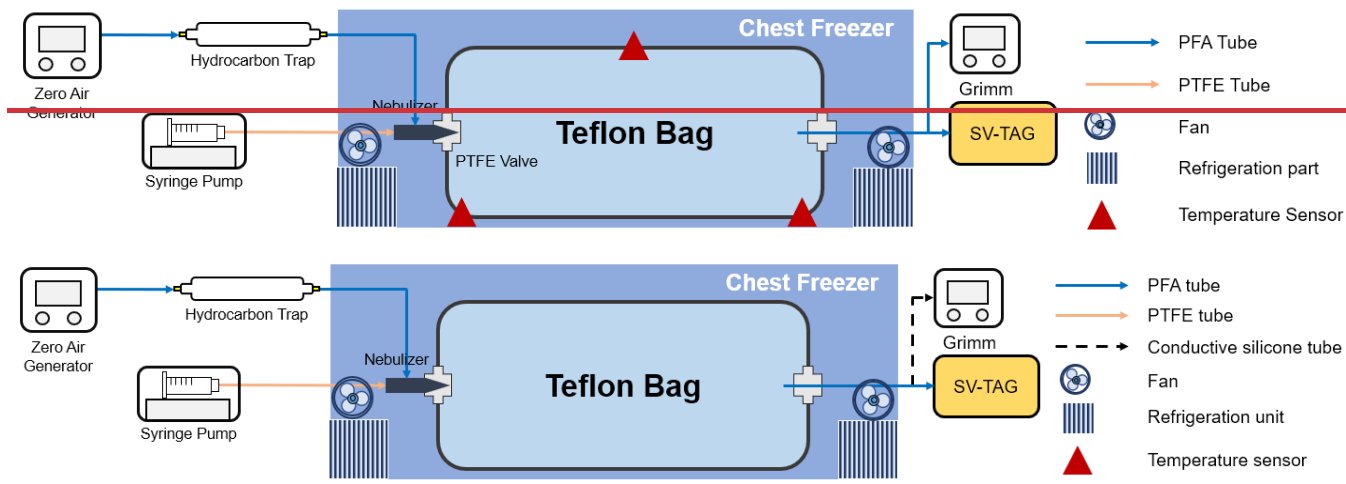
399 A table that contains the definitions of parameters and corresponding units.

400	$k_1$	forward rate constant ( $s^{-1}$ )
401	$k_{-1}$	backward rate constant ( $s^{-1}$ )
402	$k_2$	first-order loss rate constant ( $s^{-1}$ )
403	$\tau_{surface}$	gas-surface equilibrium time scale (min)
404	$\tau_{inner}$	diffusion time scale (min)
405	$C_0$	initial SVOC concentration in gas phase ( $\mu\text{g m}^{-3}$ )
406	$C_{gas}$	SVOC concentration in gas phase ( $\mu\text{g m}^{-3}$ )
407	$C_{wall}$	SVOC concentration on wall surface ( $\mu\text{g m}^{-3}$ )
408	$K_{eq}$	gas-surface equilibrium constant
409	$C_{FEP\_surface}$	equivalent organic mass concentration of the FEP chamber surface ( $\text{mg m}^{-3}$ )
410	$M_{wall}$	average molecular mass of the Teflon wall ( $\text{g mol}^{-1}$ )
411	$\gamma_{FEP\_surface}$	activity coefficient in the Teflon surface
412	$R$	gas constant ( $\text{J K}^{-1} \text{mol}^{-1}$ )
413	$T$	temperature (K)
414	$P_s(T)$	saturation vapor pressure of compound at temperature $T$ (Pa)

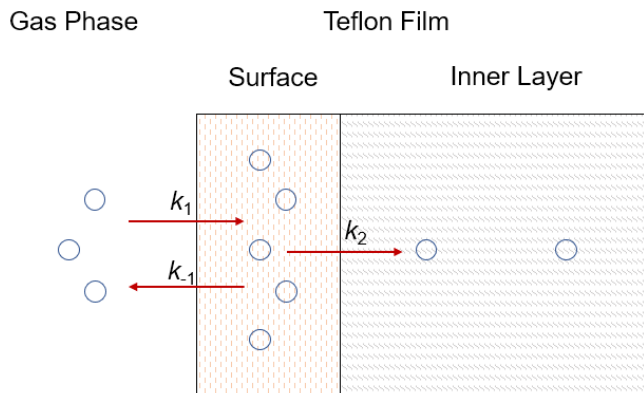


415

416

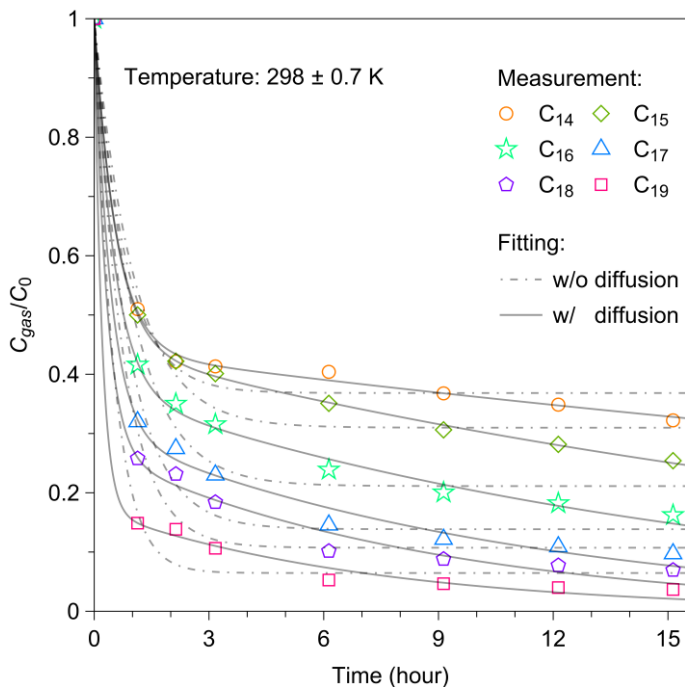


417 **Figure 1.** Schematic diagram of the experimental setup.



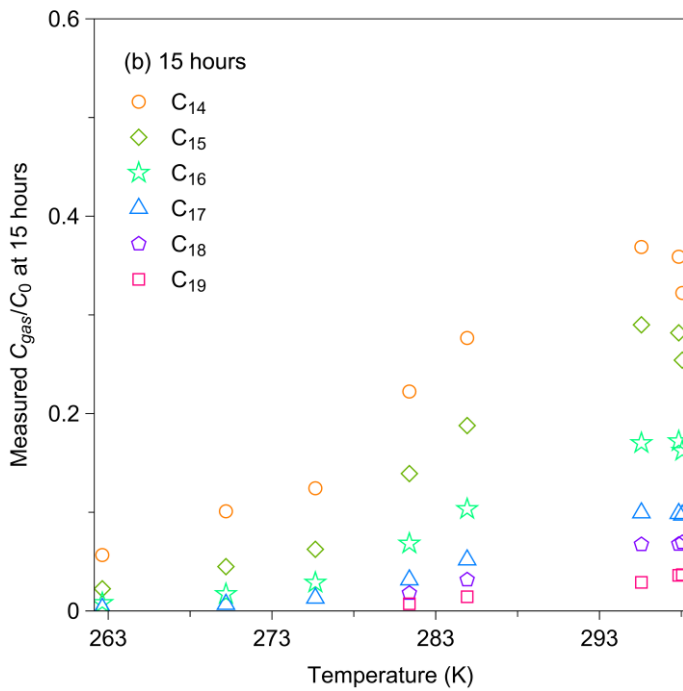
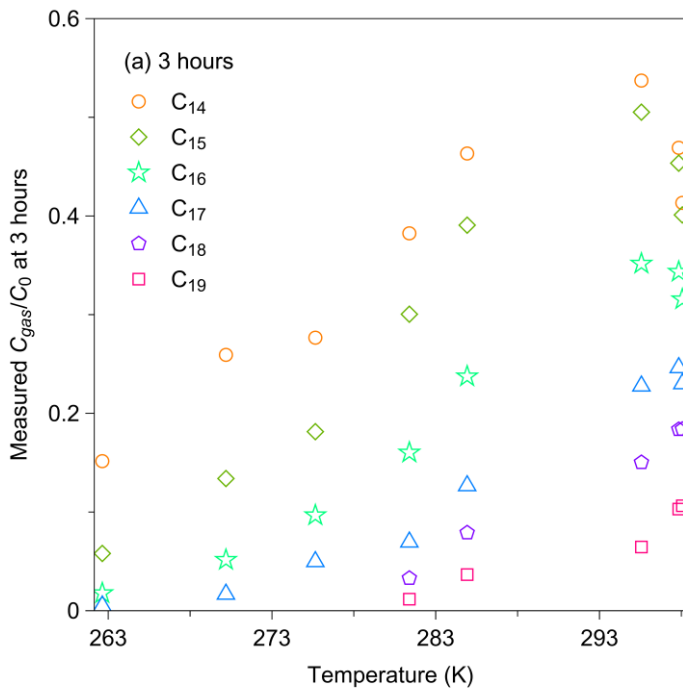
418

419 **Figure 2.** Schematic diagram of wall loss process. Compounds partition between gas phase and surface layer with forward  
420 and backward rates ( $k_1$  and  $k_{-1}$ ). Compounds in surface layer undergo irreversible diffusion into inner layer with first-order  
421 loss rate ( $k_2$ ).



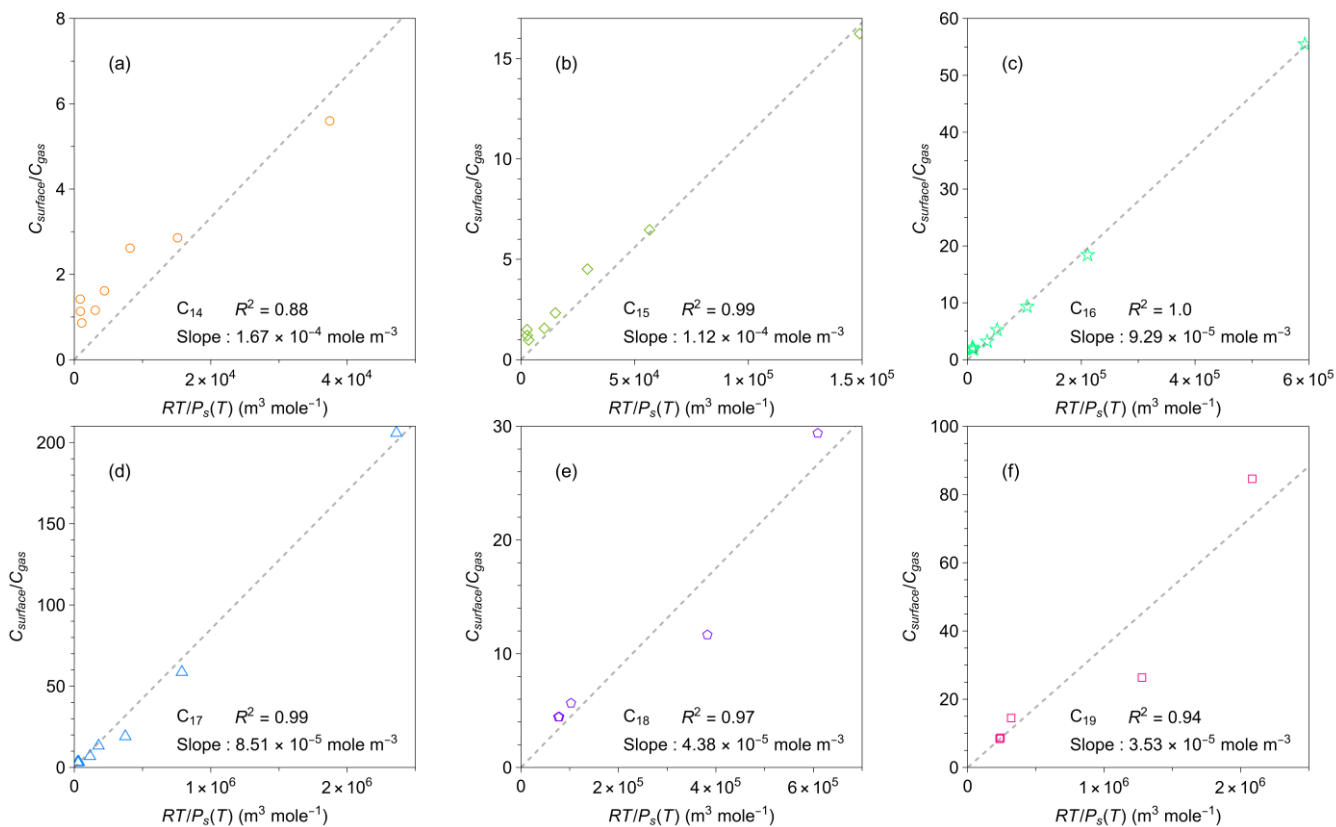
422

423 **Figure 3.** Temporal variation in  $C_{gas}/C_0$  for  $C_{14}$ - $C_{19}$   $n$ -alkanes at  $298 \pm 0.7$  K following injection.  $C_{gas}$  is the concentration of  
 424 each  $n$ -alkane in the gas phase, and  $C_0$  is the corresponding initial concentration of each  $n$ -alkane. The two-layer kinetic  
 425 sorption model (Section 2.2) was employed to fit the data (black solid line). The black dot-dashed lines show the fitting result  
 426 to the model that ignores the diffusion process to the inner layer (*i.e.*,  $k_2 = 0$ ).



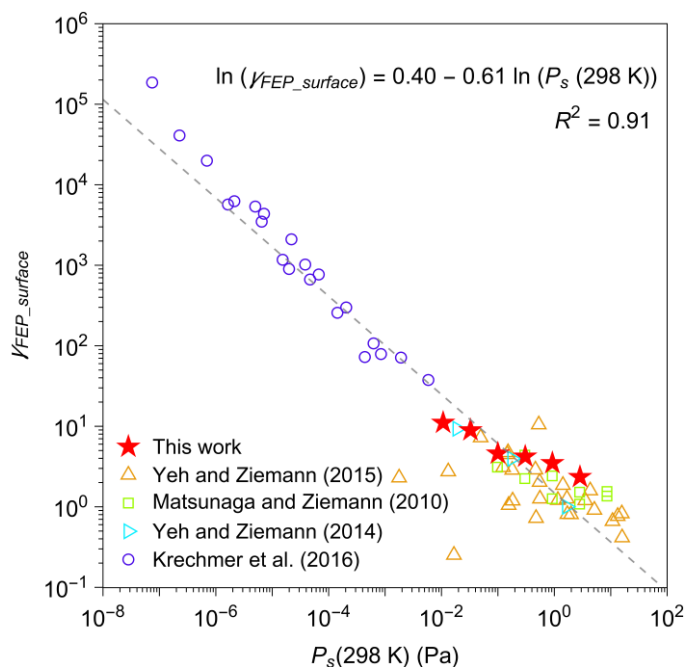
427

428 **Figure 4.** Measured values of  $C_{gas}/C_0$  at (a) 3 hours and (b) 15 hours after injection.



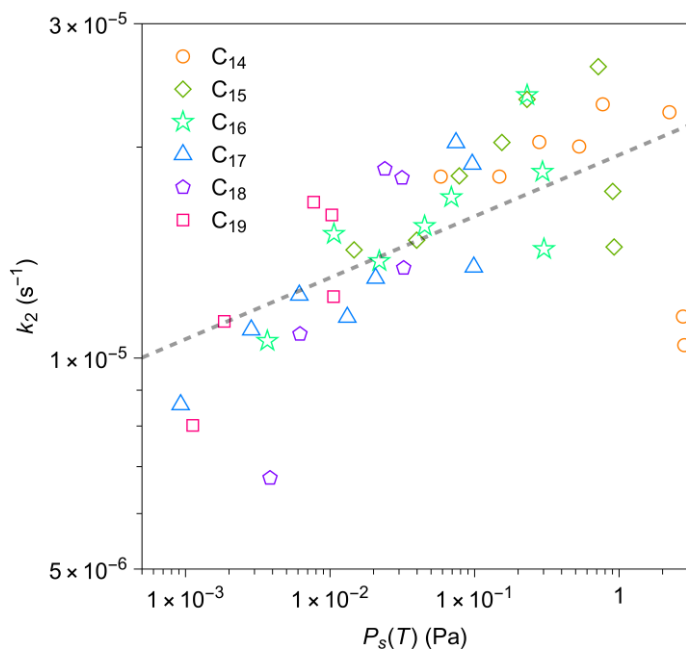
429

430 **Figure 5.** Relationships between measured ratio of concentrations in the chamber wall surface phase and in the gas phase at  
 431 quasi-equilibrium and calculated values of  $RT/P_s(T)$  for individual  $n$ -alkanes. Calculation methods for  $C_{surface}/C_{gas}$  is  
 432 detailed in the text. The values of  $RT/P_s(T)$  for each  $n$ -alkane were calculated by the EVAPORATION group contribution  
 433 method (Compernelle et al., 2011). The black dashed lines are best linear fits of linear least squares that fit the data for each  
 434  $n$ -alkane.



435

436 **Figure 6.** Activity coefficient ( $\gamma_{FEP\_surface}$ ) of organic compounds in FEP film. The sources of data include this work and the  
 437 literature (compiled by Huang et al. (2018b), including Matsunaga and Ziemann (2010), Yeh and Ziemann (2014, 2015), and  
 438 Krechmer et al. (2016)). A list of chemical species that were investigated by each study is available in Table S4. Saturation  
 439 vapor pressures at 298 K ( $P_s(298\text{ K})$ ) were estimated by EVAPORATION (Compennolle et al., 2011).



440

441 **Figure 7.** Relationship between calculated first-order loss rate  $k_2$  for each  $n$ -alkane and calculated values of saturation vapor  
 442 pressure by the EVAPORATION group contribution method (Compernelle et al., 2011). The calculation method for  $k_2$  is  
 443 detailed in the text. The black dashed line is the best linear least squares fit to the data in a logarithmic scale.